Nonequilibrium hole relaxation dynamics in an intrinsic semiconductor

P. Langot, R. Tommasi,* and F. Vallée

Laboratoire d'Optique Quantique du CNRS, Ecole Polytechnique–91128 Palaiseau Cedex, France

(Received 30 January 1996)

The thermalization dynamics of photoexcited nonequilibrium holes is selectively investigated in intrinsic bulk GaAs using a high sensitivity two-wavelength pump-probe technique. The carriers are photoexcited close to the bottom of their respective bands and hole heating is followed by monitoring the absorption saturation due to filling of higher-energy states. The characteristic thermalization time is measured to increase only slightly from ~ 120 to ~ 170 fs as carrier density decreases from 7×10^{17} to 2×10^{16} cm^{-3}, indicating that hole heating is dominated by hole–optical-phonon scattering. These results are in good agreement with a simulation of the carrier relaxation based on numerical resolution of the carrier Boltzmann equations including interaction of holes with LO and TO phonons. [S0163-1829(96)10327-1]

I. INTRODUCTION

Ultrafast relaxation dynamics of photoexcited free carriers has been extensively investigated in semiconductors, both theoretically and experimentally, yielding important information on carrier elementary scattering processes in bulk and low-dimensionality systems.[1–12] In particular, the central problem of energy redistribution and exchange processes has been studied on a femtosecond time scale using incoherent optical techniques, such as time-resolved luminescence and absorption saturation spectroscopy. These techniques are generally based on interband optical transitions and are thus *a priori* sensitive to both electron and hole relaxation. However, because of the band structure, hole relaxation is generally faster and/or its contribution to the measured signal smaller and the electron response generally dominates the measured transient signal.[12] Specific time-resolved experiments have thus to be designed to selectively access hole relaxation dynamics.[13–19] Consequently, although electron interaction processes are now relatively well characterized, little is known on hole thermalization dynamics, especially in intrinsic direct-gap semiconductors, except at very high carrier density in the gain regime.[20,21]

This problem has recently been addressed in *n*-doped bulk GaAs and InP and GaAs/Al$_x$Ga$_{1-x}$As quantum wells using time-resolved luminescence.[13,14] In these experiments, the high-density thermal electron population introduced by doping acts as a reservoir for the recombination of low-density photoexcited hot holes, permitting the determination of their cooling dynamics, but also as a thermal bath dominating hole cooling at low temperatures.[13,14] To suppress this effect, thermalization of a one-component plasma has been studied in *p*-doped Ge using a femtosecond intervalence band absorption saturation technique.[16,17] These measurements, performed at low temperature, show contributions of both scattering of nonequilibrium holes by the background thermal holes and of hole-phonon interactions.[17] In this paper, we report on the selective investigation of low-energy heavy-hole (HH) heating dynamics in an intrinsic polar semiconductor: GaAs, using a femtosecond high-sensitivity two-wavelength absorption saturation technique.

In femtosecond absorption saturation measurements a short pump pulse generates a nonequilibrium electron-hole distribution through interband absorption. The carriers, with density ρ, quickly redistribute in their respective bands and information on their transient distributions is obtained by following the temporal evolution of the differential transmission, $\Delta T/T = [T(\rho) - T(0)]/T(0)$, of a probe pulse.[3] For an antireflection coated sample, changes of the refractive index can be neglected and $\Delta T/T$ at the probe photon energy, $\hbar \omega_{pr}$, is proportional to the modification $\Delta \alpha$ of the sample absorption α ($\Delta T/T = -\Delta \alpha L$, for an optically thin sample with thickness L):

$$\alpha(\hbar \omega_{pr}, \rho) = \alpha_0 \sum_v \mu_v^{3/2} C_v(\rho, \hbar \omega_{pr}) \sqrt{\Delta E_{pr}(\rho)}$$
$$\times [1 - f_e(k_{pr}^v) - f_v(k_{pr}^v)], \qquad (1)$$

where the summation is performed over the valence bands involved (light- and heavy-hole bands in our measurements) assuming the same average optical transition amplitude.[8] $\Delta E_{pr} = \hbar \omega_{pr} - E_g(\rho)$ is the excess probe photon energy relative to the carrier density dependent band gap, C_v is the Sommerfeld or Coulomb enhancement factor,[22] and μ_v is the reduced electron-hole mass. $f_e(k_{pr}^v)$ and $f_v(k_{pr}^v)$ are the occupation numbers of, respectively, the probed electron and hole states with wave vector $k_{pr}^v = \sqrt{2 \mu_v \Delta E_{pr}}/\hbar$. As high-energy states are probed, the excitonic terms have been disregarded. The normalized absorption change, $\Delta \alpha/\alpha$, after photoinjection of a carrier plasma in an intrinsic sample, can be written as the sum of two terms:

$$\frac{\Delta \alpha}{\alpha}(\hbar \omega_{pr}, \rho) \cong \frac{\sum_v \mu_v^{3/2} \Delta(C_v(\hbar \omega_{pr}, \rho) \sqrt{\Delta E_{pr}(\rho)})}{\sum_v \mu_v^{3/2} C_v(\hbar \omega_{pr}, 0) \sqrt{\Delta E_{pr}(0)}}$$

$$- \frac{\sum_v \mu_v^{3/2} C_v(\hbar \omega_{pr}, 0)(f_e(k_{pr}^v) + f_v(k_{pr}^v))}{\sum_v \mu_v^{3/2} C_v(\hbar \omega_{pr}, 0)}.$$

$$(2)$$
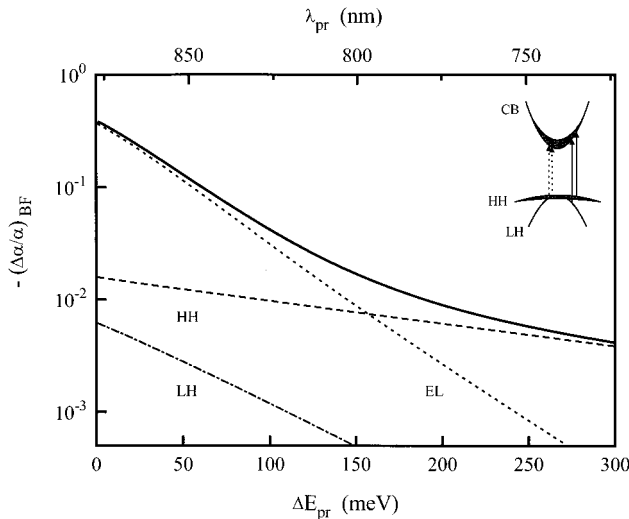
FIG. 1. Total normalized absorption change, $(\Delta\alpha/\alpha)_{BF}$ (full line), due to band filling as a function of the probe photon excess energy, $\Delta E_{pr} = \hbar\omega_{pr} - E_g$, for a thermal electron-hole plasma ($T = 295$ K) with a density of 2×10^{17} cm^{-3} in GaAs. The individual contributions due to filling of the conduction (EL), heavy-hole (HH) and light-hole (LH) bands are also shown. The excited (dashed arrow) and probed (full arrow) transitions are schematically shown in the inset.

The first one lumps the effects of the band-gap shrinkage and of the reduction of the Sommerfeld factor due to creation of carrier (many-body effects).[10,23] The second term, which corresponds to absorption saturation, is the usual band-filling (BF) contribution, $(\Delta\alpha/\alpha)_{BF}$, which contains direct information on the free carrier k-space distributions.[3] In contrast to time-resolved luminescence, where the measured signal is proportional to the product of the occupation numbers of the identical momentum electron and hole that recombine, absorption saturation spectroscopy depends on the sum of the carrier occupation numbers. Their contributions to $(\Delta\alpha/\alpha)_{BF}$ are thus intrinsically separated and experimental conditions can be chosen so that this term is dominated by either the electron or hole band-filling effect.

Because of the large HH-electron mass ratio, the root-mean-square momentum of a thermal HH distribution is much larger than that of the corresponding electron distribution. Consequently, for small wave vectors, the electron occupation number is much larger than the HH one and $(\Delta\alpha/\alpha)_{BF}$ is essentially due to occupation of the conduction-band states when probing close to the band edge. In contrast, for large wave vectors (i.e., large ΔE_{pr}), the probed hole occupation number is larger than the electronic one and heavy holes give the dominant contribution to $(\Delta\alpha/\alpha)_{BF}$. The existence of these two regimes is clearly shown in Fig. 1 where $(\Delta\alpha/\alpha)_{BF}$ and the relative contributions due to filling of the electron (EL), light hole (LH), and HH states are plotted as a function of ΔE_{pr}, for a thermal electron-hole plasma ($T = 295$ K) in GaAs. The carrier density is 2×10^{17} cm^{-3} and the Elliot formula has been used for $C_v(\hbar\omega_{pr},0)$.[24] For ΔE_{pr} larger than ~ 200 meV (i.e., $\lambda_{pr} \lesssim 770$ nm) the absorption change is essentially due to filling of the HH states. In that range, electrons are essentially probed from the LH band, the higher-energy conduction-band states probed from

the HH band having a much smaller occupation number. Filling of the LH states is always negligible, most of the holes ($\sim 95\%$) being in the HH band at thermal equilibrium.

The different carrier contributions to $(\Delta\alpha/\alpha)_{BF}$ were computed assuming isotropic parabolic conduction and valence bands. The HH band anisotropy might modify the above description and its effect has been estimated by calculating the relative contributions to $(\Delta\alpha/\alpha)_{BF}$ for different HH masses. $(\Delta\alpha/\alpha)_{BF}$ for large ΔE_{pr} has been found to be always dominated by HH band filling, the ratio of the HH contribution to the electron one changing, for instance, from ~ 5.5 to ~ 4.5 as m_{HH} is changed from $0.35m_0$ (m_{HH} along the X direction) to $0.91m_0$ (m_{HH} along the L direction) for $\Delta E_{pr} = 250$ meV.

In the nonequilibrium case, the electrons can be confined to small momentum states by photoexciting them with an average momentum of the order or smaller than the thermal one (i.e., $\lambda_{pp} \gtrsim 840$ nm at 295 K). In these conditions, as most of the excess energy is injected into the electron system, the initial average hole energy is smaller than the thermal one and the heating dynamics of cold holes is investigated by probing large momentum states. This conclusion will be confirmed by computing the different transient band-filling contributions to $\Delta\alpha/\alpha$ in more detail in Sec. II for nonequilibrium photoexcited carriers. The results of the calculations will be compared to the experimental measurements in Sec. IV.

II. NUMERICAL SIMULATIONS

The dynamics of the photoexcited carriers is modeled using a global description considering only energy redistribution processes and neglecting coherent effects.[25] These are expected to only weakly alter the measured signal for the carrier densities ($\geq 2 \times 10^{16}$ cm^{-3}) and high-energy carrier states investigated here. The nonequilibrium distributions are described by the wave-vector-dependent occupation numbers, f_i, of the different bands whose time evolutions are computed by numerically solving the carrier Boltzmann equations:

$$\frac{df_i(\mathbf{k})}{dt} = \left(\frac{df_i(\mathbf{k})}{dt}\right)_j + \left(\frac{df_i(\mathbf{k})}{dt}\right)_{phonons} + g_i(\mathbf{k},t). \quad (3)$$

i,j stand for the electron, heavy-hole, and light-hole bands, and g_i is a photoinjection function determined by the pump pulse. $(df_i/dt)_j$ describes scattering of i carriers by j carriers and $(df_i/dt)_{phonons}$ the energy exchanges between phonons and i carriers. Assuming isotropic parabolic bands (with effective masses $m_e = 0.066m_0$, $m_{HH} = 0.5m_0$, $m_{LH} = 0.082m_0$) and neglecting the transient k-space anisotropy of the carrier distributions,[2,6] the occupation numbers only depend on the carrier energy, which greatly simplifies resolution of the above system,[25,26] making it manageable on a personal computer.

The carrier-carrier scattering rates are identical to those extensively discussed by many authors,[25,27–30] neglecting the exchange term, and will not be explicitly given here. For scattering processes involving holes, the zone center hole wave function overlap integrals calculated by Wiley[31] have been taken into account in the Coulomb matrix elements.

Intervalence band scattering induced by carrier-carrier interactions has been neglected. Screening of the carrier Coulombic interactions has been treated statically but its dynamic character has been partly taken into account by considering only screening by identical or lighter carriers than those involved in the scattering. This approximation, frequently used in Monte Carlo simulations, gives a good description of screening for electrons.[8,29,32] Underestimation of hole-hole scattering rates using static screening is expected to be less stringent than for electrons because of the larger momentum exchange for a given energy exchange.[30]

Polar and nonpolar holes–optical-phonon scattering has been considered for both intraband and interband processes and measurements being performed at room temperature; carrier acoustic phonon scattering has been disregarded.[33] As absorption and emission of LO phonons is accompanied by a large momentum exchange, the static approximation gives a good description of screening of the polar interaction for densities up to 10^{18} cm^{-3} and has been used here.[30] The intraband polar scattering rates are given in Ref. 27. The polar interband hole scattering rate from the i to j band with LO phonon emission γ_- and absorption γ_+ are calculated to be

$$\gamma_{\mp} = \frac{3e^2\omega_{LO}m_f}{32\pi\varepsilon_0\hbar^2\sqrt{2m_iE}}\left(\frac{1}{\varepsilon(\infty)} - \frac{1}{\varepsilon(0)}\right)\left[6\beta_{\mp} - 4\alpha_{\mp}\right.$$
$$\left. + (1+2\alpha_{\mp}\beta_{\mp} - 3\beta_{\mp}^2)\ln\left|\frac{\beta_{\mp}+1}{\beta_{\mp}-1}\right|\right]\left(\frac{1}{2}\pm\frac{1}{2}+n_{LO}\right),$$

$$(4)$$

where

$$\alpha_{\mp} = \frac{m_iE + m_f(E\mp\hbar\omega_{LO})}{2\sqrt{m_im_fE(E\mp\hbar\omega_{LO})}},$$

$$\beta_{\mp} = \alpha_{\mp} + \frac{\hbar^2q_D^2}{4\sqrt{m_im_fE(E\mp\hbar\omega_{LO})}}. \quad (5)$$

E is the initial hole state energy, n_{LO} the LO phonon occupation number, and q_D the Debye-Hückel wave vector:

$$q_D^2 = \frac{e^2}{\sqrt{2}\,\pi^2\varepsilon_\infty\hbar^3}\sum_i m_i^{3/2}\int_0^\infty \frac{f_i(E)}{\sqrt{E}}dE. \quad (6)$$

Nonpolar interactions with TO and LO phonons significantly contribute to the total hole-phonon scattering rate[34,35] and both intra- and inter-valence-band processes have been included. Furthermore, because of the different energy of the TO and LO phonons, multiple scattering contributes to energy redistribution between holes, especially at low densities. The nonpolar scattering rates were derived by Costato and Reggiani[36] and we have used the measured optical deformation potential $d_0 = 48$ eV.[37]

As the electron–LO phonon interaction involves small wave-vector exchanges and, for the investigated carrier density range, is thus sensitive to the screening model, dynamic screening in the plasmon pole approximation has been used.[22,30] However, this contribution does not play an essential role here since the photoexcited electrons exchange little energy with LO phonons to thermalize. For the same reason, the nonequilibrium phonon effect due to electron-phonon interactions[25,28] has been neglected.

The possible transient modification of the LO and TO phonon distributions (''cold-phonon'' effect[38]) due to phonon absorption by the cold holes has also been disregarded.[39] This is justified by the fact that because of their large mass, HH interact with large momentum (i.e., large density of states) phonons over a k-space domain that is strongly broadened by the band anisotropy. The optical phonons coupled with holes thus constitute a high heat capacity reservoir, which is expected to be only weakly perturbed by hole heating in contrast to what has been observed for cold electrons at room temperature.[34] Note that computation of the ''cold-phonon'' effect on hole heating is not straightforward and requires inclusion of a realistic warped band structure model, the isotropic approximation strongly limiting the phonon k-space domain coupled with holes and leading to a large overestimate of the effect.

The computed HH and LH transient carrier distributions are shown in Figs. 2 and 3 for a final carrier density of 2×10^{17} cm^{-3} injected by a Gaussian 70-fs pulse. The pump photon energy is $\hbar\omega_{pp}\sim1.48$ eV ($\lambda_{pp}\sim840$ mn) photoexciting electrons with an initial average excess energy of ~40 meV, close to the thermal energy at room temperature ($E_{th}\sim38$ meV). About $\frac{2}{3}$ ($\frac{1}{3}$) of the holes are created in the HH (LH) band with an excess energy of ~6 meV (~22 meV). The initial average hole excess energy is thus much lower than E_{th} and the photoexcited cold holes absorb energy to thermalize with the rest of the sample. For HH, phonon replicas are observed at early times as holes quickly absorb LO phonons. These structures are washed out by hole-hole scattering that internally thermalizes the HH distribution, which is in thermal equilibrium with the lattice for times longer than ~800 fs (Fig. 2). The light holes are quickly scattered into the heavy-hole band, mostly by optical phonon absorption (they are excited below the thresholds for optical phonon emission) resulting in a short time delay replica around 60 meV in the HH distribution. Note that LH contain most of the initial hole excess energy and efficiently heat up the cold HH. Their inclusion into the simulation is thus essential for describing hole thermalization. The initial average excess energy of the electrons being close to E_{th}, the calculated transient electron distributions show fast internal (by electron-electron scattering) and external thermalizations (Fig. 4).

The HH thermalization dynamics can be observed using a probe photon energy larger than ~1.6 eV. The energies of the probed states are indicated by the arrows in Figs. 2 and 3 for $\hbar\omega_{pr}\sim1.65$ eV ($\lambda_{pr}\sim750$ nm). To compute the total absorption change (2), renormalization of the band gap and of the optical interactions by the many-body Coulomb effect have to be calculated for the transient carrier distributions. Band-gap renormalization can be written as the sum of a Coulomb hole term and a screened exchange term as calcu-
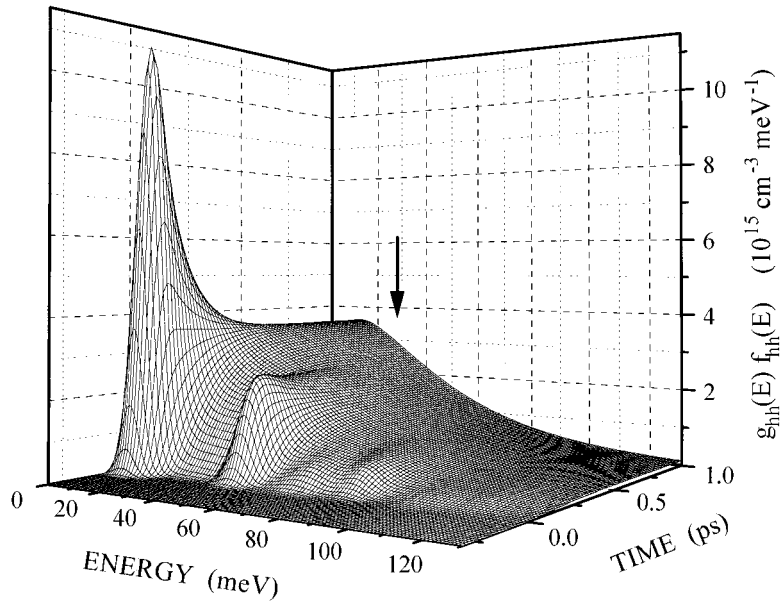
FIG. 2. Calculated transient heavy-hole distribution, $f_{HH}(E)$, times the density of heavy-hole states $g_{HH}(E)$. Heavy holes are photoexcited with an excess energy of ~ 6 meV by a 70-fs pump pulse ($\hbar \omega_{pp} = 1.48$ eV). The carrier density is 2×10^{17} cm^{-3}. The arrow indicates the probed states for a probe photon energy of 1.65 eV.

lated using a quasistatic model.[22] Assuming a rigid band shift, the band-gap energy reads

$$E_g(\rho) = E_g(0) + \sum_{\mathbf{q}} [V_{sc}(\mathbf{q}) - V_0(\mathbf{q})] - \sum_{i,\mathbf{q}} V_{sc}(\mathbf{q}) f_i(\mathbf{q}), \quad (7)$$

where V_0 and V_{sc} are the unscreened and statically screened Coulomb potentials. The modification of the optical transition matrix elements by Coulomb correlation is estimated using the analytic expression of the Coulomb enhancement factor derived for a Hùlthen potential:[22]

$$C_v(\rho) = \frac{2\pi}{\sqrt{\Delta E_{pr}/R_v}} \frac{\sinh(\pi g \sqrt{\Delta E_{pr}/R_v})}{\cosh(\pi g \sqrt{\Delta E_{pr}/R_v}) - \cos(\pi \sqrt{4g - g^2 \Delta E_{pr}/R_v})}, \quad (8)$$

where R_v is the exciton Rydberg energy and $g = 1/q_D a_B$. To derive this expression, band-filling effects have been neglected, assuming that screening gives the dominant contri-

bution. The nonequilibrium nature of the plasma is thus only reflected in the distribution-dependent Debye-Hückel wave vector. Note that this expression reduces to the Elliot for-
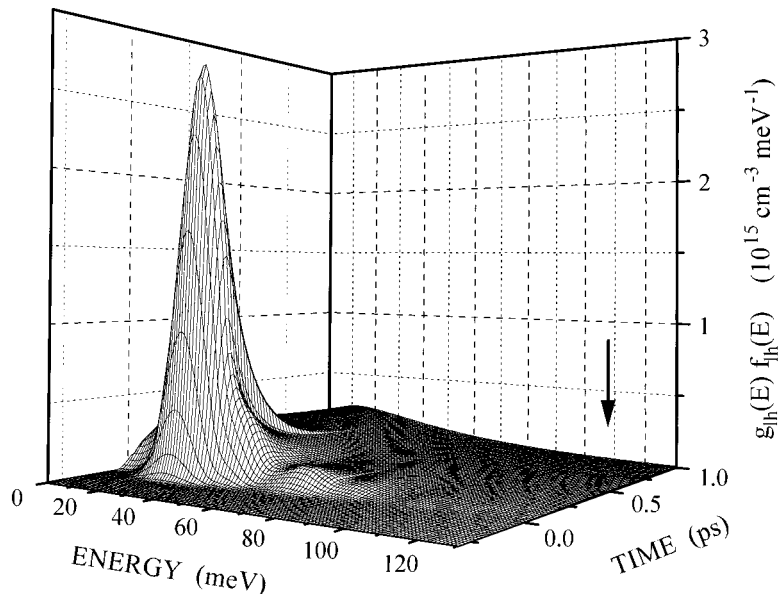
FIG. 3. Calculated transient light-hole distribution, $f_{LH}(E)$, times the density of light-hole states $g_{LH}(E)$ for the same conditions as Fig. 2. The light-hole initial excess energy is ~ 22 meV. The arrow indicates the probing position for a probe photon energy of 1.65 eV.
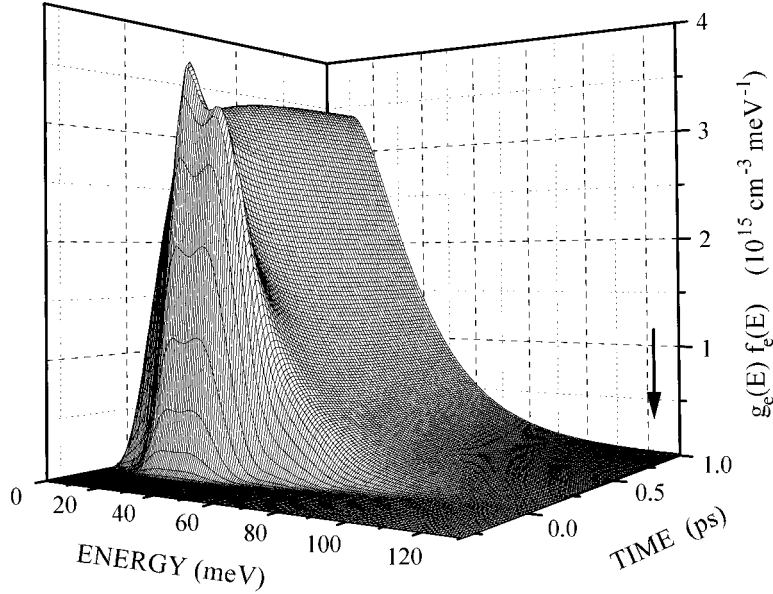
FIG. 4. Calculated transient electron distribution, $f_e(E)$, times the density of states $g_e(E)$ for the same conditions as Fig. 2. The two peaks correspond to photoexcitation from the heavy- and light-hole bands. The arrow indicates the states probed from the light-hole band for a probe photon energy of 1.65 eV.

mula for vanishing carrier densities.[24]

The calculated transmission change is shown in Fig. 5 for $\rho = 2 \times 10^{17}$ cm^{-3}, together with the individual contributions due to filling of the electron and hole states and to many-body effects. Because of the large momentum difference between the probed and photoexcited states, BF effects are delayed and the short time delay signal is mainly due to the many-body effects. Increase of the probed density of states (and thus of the absorption) by band-gap renormalization predominates over reduction of the Coulomb enhancement (that reduces the absorption) resulting in an almost instantaneous decrease of the sample transmission. This contribution depends on carrier density but, in our experimental conditions, is only weakly sensitive to the exact carrier distributions. It is thus almost constant after carrier injection has terminated, resulting in a signal offset. These results are consistent with recent Monte Carlo simulations for nonequilib-

rium distributions photoexcited close to the band edge.[9] The subsequent rise of $\Delta T / T$ is mainly due to filling of the probed HH states as the initially cold distribution heats up and thermalizes (direct contribution due to filling of the LH states is negligible). As expected (Fig. 1), the electrons only weakly contribute to the total signal.
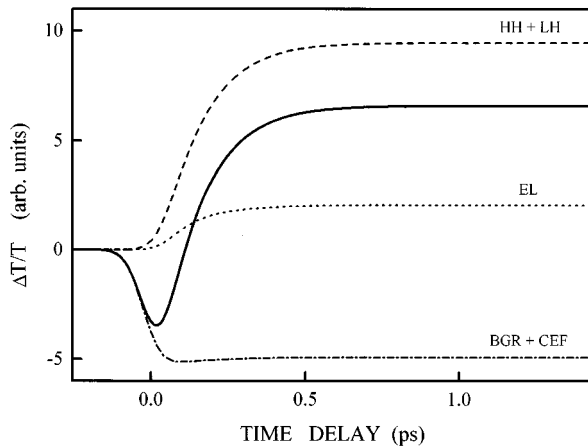
The carrier occupation numbers changing linearly with carrier density at thermal equilibrium for nondegenerate distributions, similar relative amplitudes of the band-filling contributions are computed for lower densities. For larger densities ($\rho \geq 5 \times 10^{17}$ cm^{-3}), the electron distribution becomes significantly degenerated and its contribution increases, partly masking the hole thermalization dynamics (see Sec. IV).

III. EXPERIMENTAL SYSTEM

To perform high sensitivity two-color femtosecond pump-probe measurements, we have developed a high repetition rate source generating synchronized independently tunable pulses by nonlinear frequency conversion of a Kerr-lens mode-locked Ti:sapphire laser.[40] The laser is operated at 800 nm and its output is passed through a Faraday isolator. After external group velocity dispersion compensation in a prism pair, the pulse duration is 50 fs with an average power of 1.2 W. The pulse train is then coupled into a 5.5-cm-long, 3.9-μm core diameter single mode optical fiber where self-phase modulation broadens the spectrum from ~ 14 to ~ 130 nm (full width at half maximum). The output of the fiber (~ 600 mW) is then split into two parts, which are independently temporally compressed and spectrally filtered using two identical grating pair systems to generate two synchronized frequency tunable femtosecond pulses. Each system consists of two diffraction gratings separated by a unity magnification telescope.[29] Wavelength selection is performed using an adjustable slit placed out of the Fourier plane, which permits generation of nearly Gaussian pulses.[41] The width of the slits is adjusted to produce transformed limited 70-fs pulses with a maximum average power of 20 mW. Using the wings of the spectrum, pulses separated by as much as 170

FIG. 5. Calculated transient transmission change, $\Delta T / T$ (full line) for a pump (probe) photon energy of 1.48 eV (1.65 eV) and a carrier density of 2×10^{17} cm^{-3}. The individual contributions to $\Delta T / T$ due to band-gap renormalization and reduction of the Coulomb enhancement factor (BGR+CEF) and to filling of the conduction (EL) and valence bands (HH+LH) are also shown.
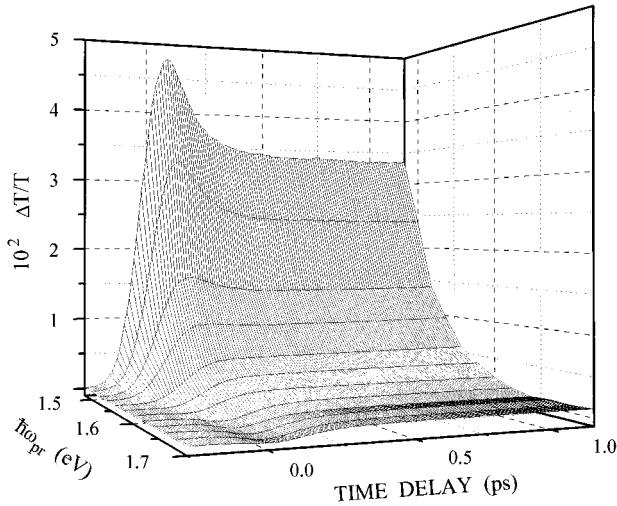
FIG. 6. Measured transient transmission change in GaAs for a pump photon energy of 1.48 eV and a probe photon energy ranging from 1.48 to 1.7 eV. The carrier density is 3×10^{17} cm^{-3}.

FIG. 7. Measured transient transmission change $\Delta T/T$ in GaAs for pump and probe photon energies of respectively 1.48 and 1.65 eV. The photoexcited carrier density is $\sim 2 \times 10^{17}$ cm^{-3}. The inset shows the corresponding normalized transmission change difference, NDT=$[(\Delta T/T)_M - \Delta T/T]/(\Delta T/T)_M$ on a logarithmic scale as a function of the probe time delay [$(\Delta T/T)_M$ is the quasiequilibrium transmission change measured for $t=1$ ps].

nm can be created with a tunable central wavelength. This source offers many possibilities for two-color femtosecond spectroscopy when limited tunability and peak power are required and is particularly well adapted to the investigation of semiconductor systems.

The two beams are sent into a standard pump-probe setup. The probe beam is passed through a variable delay stage and cross polarized with the pump. The beams are focused into the sample using a $10\times$ microscope objective. The focal spot size has been measured to be 15 μm in diameter by imaging the sample with a microscope onto a CCD camera. Measurements were performed at room temperature in a 0.2-μm-thick GaAs sample with Al$_{0.6}$Ga$_{0.4}$As cladding layers and antireflection coating. The pump beam is chopped at 1.5 kHz and the signal is detected using a lock-in amplifier. The high stability of the laser and the high repetition rate of the tunable pulses (76 MHz) permit very high sensitivity measurements with a noise level for $\Delta T/T$ in the 10^{-6} range.

IV. RESULTS AND DISCUSSION

The results of the measurements are shown in Fig. 6 for a pump photon energy of 1.48 eV ($\lambda_{pp} \sim 840$ nm) and probe photon energies ranging from 1.48 to 1.70 eV (840 nm $\geqslant \lambda_{pr} \geqslant 730$ nm). For small $\hbar\omega_{pr}$ the measured temporal behavior is dominated by the electron thermalization dynamics (Fig. 1) and exhibits a fast short time delay response resulting from the partial overlap of the excited and probed electron and hole states (hole burning[3]). As the electrons are excited with an excess energy close to the average energy at room temperature, they quickly thermalize between themselves and with the lattice leading to a fast decay of the transient induced transmission. The hole burning effect is reduced as the probe photon energy increases and for $\hbar\omega_{pr} \geqslant 1.6$ eV ($\lambda_{pr} \leqslant 770$ nm), the temporal behavior is drastically modified (Fig. 6) with a fast short time delay transmission decrease followed by a slow rise and a plateau. The amplitude of the long term ($t=1$ ps) transmission change is strongly reduced from $\Delta T/T \sim 3.3 \times 10^{-2}$ for identical pump

and probe wavelengths to $\Delta T/T \sim 1.2 \times 10^{-3}$ for $\lambda_{pr} \sim 750$ nm ($\hbar\omega_{pr} \sim 1.65$ eV) consistent with the ~ 10 time reduction of the band-filling effect calculated at thermal equilibrium at room temperature (Fig. 1). A larger reduction is measured because of the transmission decrease induced by many-body effects, which weakly affect $\Delta T/T$ for probing closer to the band edge ($\hbar\omega_{pr} \sim 1.5$ eV) but significantly contribute for high probe photon energies (Fig. 5). For larger $\hbar\omega_{pr}(\geqslant 1.72$ eV, i.e., $\lambda_{pr} \leqslant 720$ nm), the temporal shape of the measured $\Delta T/T$ changes and its long-term amplitude increases as a result of the onset of probing the bottom of the conduction band from the spin split-off valence band. Information on hole thermalization dynamics is thus contained in the intermediate region (1.6 eV$\leqslant \hbar\omega_{pr} \leqslant 1.7$ eV) where electron dynamics plays a minor role.

The measured temporal behavior is shown on an enlarged scale in Fig. 7 for $\hbar\omega_{pr} \sim 1.65$ eV and $\rho \sim 2 \times 10^{17}$ cm^{-3}. Transient reflectivity measurements performed simultaneously show that the change of the real part of the sample refractive index does not significantly contribute to the measured $\Delta T/T$, which can thus be directly related to the absorption change $\Delta\alpha$. The measured dynamics is comparable to the calculated one (Fig. 5) with a short time delay signal dominated by band-gap renormalization (BGR). The transmission change reaches a plateau after ~ 700 fs, indicating that heavy holes are in quasiequilibrium with the rest of the sample, in good agreement with the computed transient carrier distributions (Fig. 2). Similar temporal behavior were measured for probe wavelengths in the region dominated by the hole dynamics.

Measurements performed for carrier densities ranging from 2×10^{16} to 1×10^{18} cm^{-3} show comparable temporal behaviors (Fig. 8 for $\hbar\omega_{pr} \sim 1.63$ eV, i.e., $\lambda_{pr} \sim 760$ nm), with a reduction of the relative amplitude of the transient transmission decrease with increasing carrier density. This is a consequence of the fact that BGR scales sublinearly with
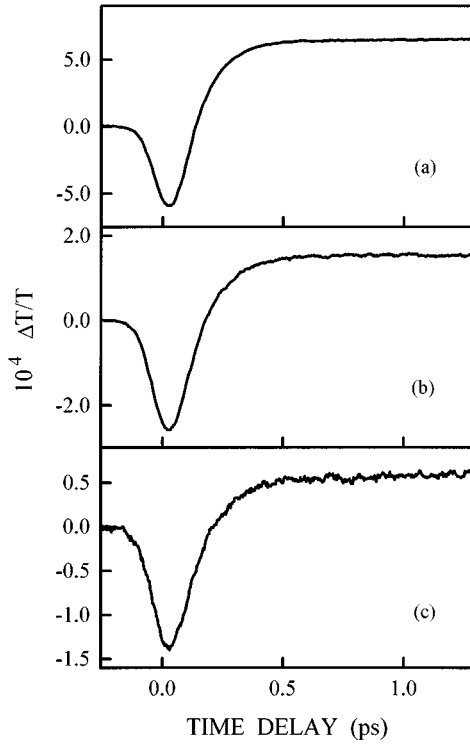
FIG. 8. Measured transient transmission change in GaAs for a photoexcited carrier density of (a) 2×10^{17} (b) 7×10^{16} cm^{-3}, and (c) 3×10^{16} cm^{-3}. The pump (probe) photon energy is 1.48 eV (1.63 eV).

density while band filling scales linearly for the nondegenerate hole distributions investigated here. The amplitude of the absorption increase due to BGR is thus reduced compared to the absorption decrease due to BF with increasing carrier densities, in good agreement with our simulations (Fig. 9). For moderate carrier densities ($\rho < 1 \times 10^{18}$ cm^{-3}) the signal rise is only weakly modified, indicating a small density dependence of the hole thermalization.

In order to analyze this dependence more quantitatively, we have fitted out results assuming an instantaneous transmission reduction (Fig. 5) and a monoexponential signal rise with a characteristic thermalization time, τ_{th}.[20] The phenomenological response function $R(t)$ that is convoluted with the pump-probe correlation function then reads

$$R(t) = u(t)\{-A + B[1 - \exp(-t/\tau_{th})]\}, \qquad (9)$$

where $u(t)$ is the unit step function. The validity of this approach is demonstrated in the inset of Fig. 7, clearly showing the quasiexponential decrease of the normalized transmission change difference (NDT), NDT$=[(\Delta T/T)_M - \Delta T/T]/(\Delta T/T)_M$, where $(\Delta T/T)_M$ is the quasiequilibrium differential transmission measured at $t = 1$ ps [using (9), NDT is proportional to $\exp(-t/\tau_{th})$ for t larger than the pulse duration]. The measured τ_{th} are almost constant for carrier densities larger than $\sim 6 \times 10^{16}$ cm^{-3} ($\tau_{th} \sim 130 \pm 15$ fs) and only weakly increase for lower carrier densities up to ~ 175 fs for $\rho \sim 2 \times 10^{16}$ cm^{-3} (Fig. 10). The thermalization times τ_{th} estimated from the calculated $\Delta T/T$ using the same procedure are shown by the full line in Fig. 10, in good agreement with the measured one, showing in particular a
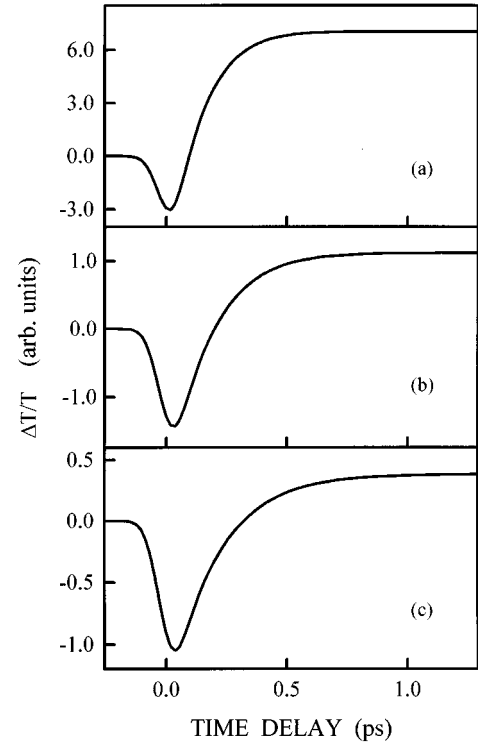
FIG. 9. Calculated transient transmission change in GaAs in the same conditions as in Fig. 8.

similar carrier density dependence. The calculated τ_{th} are slightly larger (about 10%) than the measured ones. A possible origin of this discrepancy lies in the assumption of an isotropic parabolic HH band that modifies the HH density of states and thus the computed scattering rates. The use of statically screened hole interactions, which overestimates the reduction of the scattering rate by screening[42] and the neglect of the interband scattering induced by carrier-carrier
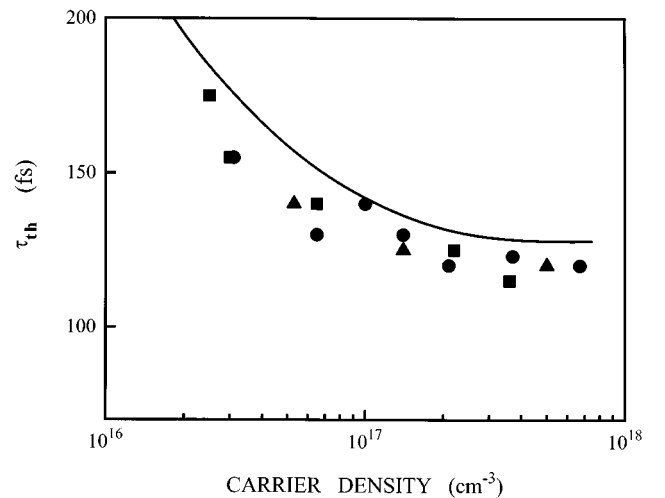
FIG. 10. Carrier density dependence of the measured and calculated (full line for $\lambda_{pr} = 750$ nm) characteristic hole thermalization times, τ_{th}, in GaAs at room temperature. The pump wavelength is 840 nm ($\hbar \omega_{pp} \sim 1.48$ eV) and the probe wavelength 760 nm ($\hbar \omega_{pr} \sim 1.63$ eV, squares), 750 nm ($\hbar \omega_{pr} \sim 1.65$ eV, points) and 740 nm ($\hbar \omega_{pr} \sim 1.68$ eV, triangles).

interactions[43] may also play a role.

The energy source for hole heating might be both the lattice and the simultaneously photoexcited electrons. However, the energy stored into the electron system being limited, a large electron-hole energy transfer would thermalize the two systems at a temperature lower than the lattice one. Energy absorption from the lattice is thus always necessary to fully thermalize the system. This is in contrast with the case of n-doped samples where with measurements being performed for doping densities much larger (~ 10 times) than the photoexcited plasma density, the thermal electrons introduced by doping can be considered as a thermal bath for holes.[13,14]

The weak dependence of the measured hole relaxation rate on carrier density and its monoexponential behavior suggest that in intrinsic systems, electron-hole scattering is not the main hole heating process and that hole thermalization is essentially due to hole–optical phonon scattering with a dominant contribution from polar interactions. LO phonon absorption by cold holes involves large momentum exchanges (for instance, holes at the top of the valence band can only exchange a momentum of $\sqrt{2m_{HH}\hbar\omega_{LO}}/\hbar$) and, in contrast to the electron–LO phonon interaction and to hot-carrier cooling processes, it is thus only weakly reduced by screening in the investigated carrier density range. In our measurements, HH states with energies ranging from ~ 23 to ~ 33 meV ($730 \leqslant \lambda_{pr} \leqslant 770$ nm), between the initial excitation peak and the first optical phonon replica, are probed (Fig. 2). The measured absorption change thus depends on both the phonon absorption rate by holes and on the hole internal thermalization time. For large densities, hole-hole scattering quickly establishes a hole temperature and τ_{th} is limited by external energy transfer from the lattice. The TO and LO phonon absorption rate by polar and nonpolar scattering has been calculated to be ~ 5 ps^{-1} at room temperature.[34] As, on the average, each hole has to increase its energy by ~ 25 meV (i.e., ~ 0.7 optical phonon) a typical thermalization time of ~ 140 fs can be roughly estimated, which favorably compare with the almost constant value of τ_{th} measured for large densities (Fig. 10).

The weak increase of τ_{th} for low densities is attributed to a slower internal thermalization of the hole distribution due to reduction of the hole-hole interactions with a small contribution from reduction of electron-hole scattering. The minor role of the electron-hole energy exchanges is consistent with the absence of any computed decrease of the electron distribution temperature (Fig. 4) that would result in a transient decrease of the electron contribution to $(\Delta\alpha/\alpha)_{BF}$ when probing the tail of the distribution (Fig. 5). Our conclusions are in agreement with numerical simulations performed for comparable excitation conditions, showing a fast LO phonon-mediated heating of holes.[10]

The role of the electrons can be further investigated by switching off the electron-hole interactions in the simulations. The results show a weak increase of the calculated τ_{th} from ~ 130 to ~ 145 fs for a carrier density of 2×10^{17} cm^{-3}. As pointed out by many authors, this slow electron-hole energy transfer that, in particular, results in a slow hole-electron thermalization on a few picosecond time scale,[20,27,44] is a simple consequence of the large HH-electron mass ratio. Furthermore, in our measurements, holes
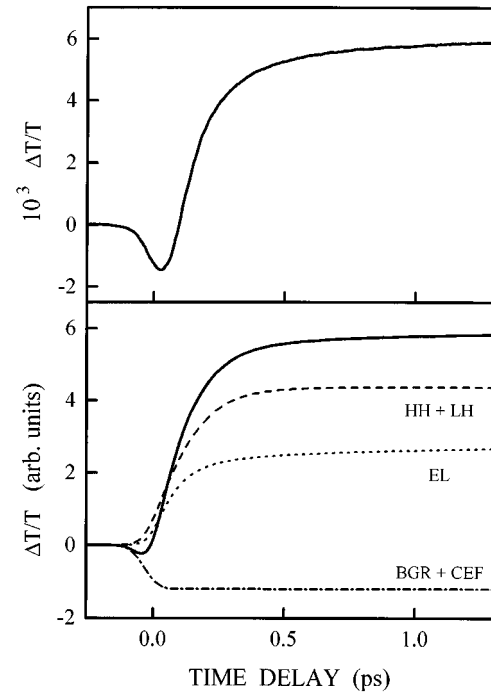
FIG. 11. Measured and calculated transient transmission change in GaAs for a photoexcited carrier density of 2×10^{18} cm^{-3} and a pump (probe) photon energy of 1.48 eV (1.64 eV). The individual contribution (labeled as in Fig. 5) to $\Delta T/T$ are also shown.

are excited close to the top of the valence band, which strongly limits the range of the possible momentum exchange for a given energy transfer. Energy and momentum conservation requirements are thus more stringent than for high-energy electrons and holes, further limiting cold hole-electron energy exchanges. Inclusion of electron-induced intervalence band scattering should slightly increase the energy transfer[43] but is not expected to drastically modify the results of the simulations. Although the initial distributions are different, the minor role played by electrons in our measurements is consistent with the longer hole cooling times attributed to thermal electron-hole interactions in n-doped bulk samples at low temperature [$\tau_{th} \sim 560$ fs for a donor density of 6×10^{17} cm^{-3} at 77 K (Ref. 14)]. The dominant role of the phonon in cold-hole heating at room temperature agrees with a hot-hole cooling dominated by phonon emission at room temperature in the doped systems.[13] Note that the different conclusions drawn at different temperatures in the doped samples[13,14] could be ascribed to the different hole–optical phonon interaction conditions, with the phonon absorption being negligible at 77 K and the cooling efficiency by phonon emission being dependent of the hole distribution. Impact ionization of neutral impurities may also play a role in the doped bulk samples.[8]

For large carrier densities ($\geqslant 10^{18}$ cm^{-3}) the measured $\Delta T/T$ exhibits an additional slowly rising component (Fig. 11) making separation of the electron and hole dynamics difficult. At these densities, the electron distribution is strongly degenerated and broadens in k space (at room temperature, the electron average thermal energy rises from ~ 38 meV for a nondegenerate distribution to ~ 69 meV for $\rho = 2 \times 10^{18}$ cm^{-3}), increasing the relative electron contribu-

tion to $(\Delta\alpha/\alpha)_{BF}$. For the pump photon energy used in our measurements (1.48 eV), cold electrons are thus photoexcited at high densities. Because of their smaller mass, electrons absorb LO phonons at a slower rate than cold holes (the absorption rate is about 2.5 times smaller) leading to a slow heatup of the cold electrons. The measured signal thus exhibits a slowly rising component that reflects cold electron–LO phonon interactions (Fig. 11). The total transmission change and its different components computed in these conditions are plotted in Fig. 11, clearly showing the increase of the relative electron contribution compared to lower densities (Fig. 5) and its different temporal behavior. Note that this slow rise further confirms the slow electron-hole thermalization. This conclusion is also in agreement with measurements performed in nondegenerate systems for cold electron and hole distributions that show a weak modification of the HH thermalization time and a comparably slow electron heatup.[45]

V. CONCLUSION

In conclusion, we have demonstrated that thermalization of holes photoexcited with an average energy smaller than the thermal one can be investigated in an intrinsic direct-gap semiconductor using a high-sensitivity two-wavelength pump-probe technique. These measurements take advantage of a higher k-space localization of electrons than heavy holes, which, together with the momentum state selectivity of the optical techniques, permits separation of the conduction- and valence-band filling contributions to the absorption saturation. Characteristic heavy-hole heating times increasing from ~ 120 to ~ 170 fs have been measured in GaAs at room temperature for carrier density varying from 7×10^{17} to 2×10^{16} cm^{-3}. Heavy-hole states with energies between the average energy and that of the first optical pho-

non replica are probed and hence the measured times reflect both internal and external hole thermalization. The weak carrier density dependence indicates that the thermalization is dominated by hole–optical phonon interactions, in agreement with simulations of the carrier dynamics based on numerical resolution of the carrier Boltzmann equations. The computed heating times are, however, slightly longer than the measured ones. More sophisticated numerical simulations including band anisotropy and dynamic screening of the hole interactions would be particularly interesting. The measured heating times are consistent with the absorption time of optical phonon by small momentum holes (including polar and nonpolar interactions), taking into account that on the average each hole absorbs less than one phonon to thermalize with the lattice.

These measurements open up many possibilities for precise and selective analysis of hole interactions with their environment in various semiconductors. The little used approach of investigating cold-carrier thermalization is particularly interesting for investigating carrier-phonon interactions. In contrast to hot-carrier cooling, heating of cold carriers by phonons is strongly dependent on the lattice temperature (the efficiency of phonon absorption is proportional to their occupation number) which should permit a quantitative separation of carrier-phonon interactions from other scattering processes. The effect of a thermal carrier background injected by doping or photoexcited by a prepulse[7,46] could also be studied and should give information on hole-hole scattering.

*Also with Dipartimento di Fisica, Università degli Studi di Bari, Via Orabona 4, I-70126 Bari, Italy.

[1] C. L. Tang and D. J. Erskine, Phys. Rev. Lett. **51**, 840 (1983).

[2] J. L. Oudar, A. Migus, D. Hulin, G. Grillon, J. Etchepare, and A. Antonetti, Phys. Rev. Lett. **53**, 384 (1984).

[3] W. Z. Lin, R. W. Schoenlein, J. G. Fujimoto, and E. P. Ippen, IEEE J. Quantum Electron. **24**, 267 (1988).

[4] P. C. Becker, H. L. Fragnito, C. H. Brito Cruz, R. L. Fork, J. E. Cunningham, J. E. Henry, and C. V. Shank, Phys. Rev. Lett. **61**, 1647 (1988).

[5] T. Elsaesser, J. Shah, L. Rota, and P. Lugli, Phys. Rev. Lett. **66**, 1757 (1991).

[6] M. T. Portella, J. Y. Bigot, R. W. Schoenlein, J. E. Cunningham, and C. V. Shank, Appl. Phys. Lett. **60**, 2123 (1992).

[7] L. H. Acioli, M. Ulman, F. Vallée, and J. G. Fujimoto, Appl. Phys. Lett. **63**, 666 (1993).

[8] U. Hohenester, P. Supancic, P. Kocevar, X. Q. Zhou, W. Kütt, and H. Kurz, Phys. Rev. B **47**, 13 233 (1993).

[9] J. E. Bair, D. Cohen, J. P. Krusius, and C. R. Pollock, Phys. Rev. B **50**, 4355 (1994).

[10] S. Hunsche, H. Heesel, A. Ewertz, H. Kurtz, and J. H. Collet, Phys. Rev. B **48**, 17 818 (1993).

[11] J. P. Foing, D. Hulin, M. Joffre, M. K. Jackson, J. L. Oudar, C. Tanguy, and M. Combescot, Phys. Rev. Lett. **68**, 110 (1992); C.

Tanguy and M. Combescot, *ibid.* **68**, 1935 (1992).

[12] C. J. Stanton, D. W. Bailey, and K. Hess, Phys. Rev. Lett. **65**, 231 (1990).

[13] X. Q. Zhou, K. Leo, and H. Kurz, Phys. Rev. B **45**, 3886 (1992).

[14] A. Chébira, J. Chesnoy, and G. M. Gale, Phys. Rev. B **46**, 4559 (1992).

[15] A. Tomita, J. Shah, J. E. Cunningham, S. M. Goodnick, P. Lugli, and S. L. Chuang, Phys. Rev. B **48**, 5708 (1993).

[16] M. Woerner, W. Frey, M. T. Portella, C. Ludwig, T. Elsaesser, and W. Kaiser, Phys. Rev. B **49**, 17 007 (1994).

[17] M. Woerner and T. Elsaesser, Phys. Rev. B **51**, 17 490 (1995).

[18] R. Tommasi, P. Langot, and F. Vallée, Appl. Phys. Lett. **66**, 1361 (1995).

[19] K. Tanaka, H. Ohtake, H. Nansei, and T. Suemoto, Phys. Rev. B **52**, 10 709 (1995).

[20] R. A. Taylor, C. W. W. Bradley, and J. F. Ryan, Solid State Electron. **32**, 1173 (1989).

[21] T. Gong, P. M. Fauchet, J. F. Young, and P. J. Kelly, Appl. Phys. Lett. **62**, 522 (1993).

[22] H. Haug and S. W. Koch, *Quantum Theory of the Optical and Electronic Properties of Semiconductors* (World Scientific, Singapore, 1993).

[23] J. H. Collet, S. Hunsche, H. Heesel, and H. Kurz, Phys. Rev. B **50**, 10 649 (1994).

[24] R. J. Elliot, Phys. Rev. **108**, 1384 (1957).

[25] J. Collet and T. Amand, J. Phys. Chem. Solids **47**, 153 (1986).

[26] D. W. Snoke, W. W. Rühle, Y.-C. Lu, and E. Bauser, Phys. Rev. B **45**, 10 979 (1992).

[27] R. P. Joshi, R. O. Grondin, and D. K. Ferry, Phys. Rev. B **42**, 5685 (1990).

[28] P. Lugli, in *Spectroscopy of Nonequilibrium Electrons and Phonons*, edited by C. V. Shank and B. P. Zakharchenya (North-Holland, Amsterdam, 1992), p. 1.

[29] M. Ulman, D. W. Bailey, L. H. Acioli, F. Vallée, C. J. Stanton, E. P. Ippen, and J. G. Fujimoto, Phys. Rev. B **47**, 10 267 (1993).

[30] J. H. Collet, Phys. Rev. B **39**, 7659 (1989); **47**, 10 279 (1993).

[31] J. D. Wiley, Phys. Rev. B **4**, 2485 (1971).

[32] L. Rota and D. K. Ferry, Appl. Phys. Lett. **62**, 2883 (1993).

[33] J. Shah and R. H. Leheny, in *Semiconductors Probed by Ultrafast Laser Spectroscopy*, edited by R. R. Alfano (Academic, New York, 1984), p. 45.

[34] T. Brudevoll, T. A. Fjeldy, J. Baek, and M. S. Shur, J. Appl. Phys. **67**, 7373 (1990).

[35] R. Scholz, J. Appl. Phys. **77**, 3219 (1995).

[36] M. Costato and L. Reggiani, Phys. Status Solidi B **58**, 461 (1973).

[37] M. H. Grimsditch, D. Olego, and M. Cardona, Phys. Rev. B **20**, 1758 (1979).

[38] P. Langot, R. Tommasi, and F. Vallée, Solid State Commun. **98**, 171 (1996).

[39] J. Shah, A. Pinczuk, A. C. Gossard, and W. Wiegmann, Phys. Rev. Lett. **54**, 2045 (1985).

[40] P. Langot, N. Del Fatti, R. Tommasi, and F. Vallée (unpublished).

[41] C. K. Sun, H. K. Choi, C. A. Wang, and J. G. Fujimoto, Appl. Phys. Lett. **62**, 747 (1993).

[42] J. R. Meyer and F. J. Bartoli, Phys. Rev. B **28**, 915 (1983).

[43] F. Young, P. Kelly, and N. L. Henry, Phys. Rev. B **36**, 4535 (1987).

[44] M. Asche and O. G Sarbei, Phys. Status Solidi B **126**, 607 (1984).

[45] R. Tommasi, P. Langot, N. Del Fatti, and F. Vallée, in Ultrafast Phenomena in Spectroscopy, edited by O. Svelto, S. De Silvestri, and G. Denardo (Plenum, New York, in press).

[46] T. Gong, K. B. Ucer, L. X. Zheng, G. W. Wicks, J. F. Young, P. J. Kelly, and P. M. Fauchet, in *Ultrast Phenomena*, edited by J. L. Martin, A. Migus, G. A. Mourou, and A. H. Zewail (Springer-Verlag, New York, 1993), p. 402.